Molecular Spectroscopy Workbench

Exploring Resonance Raman Spectroscopy

The scope of this work is to provide you with an overview of the chemical physics of resonance Raman spectroscopy, present and discuss some examples of resonance Raman spectra, and discuss those things to be alert to in recognizing resonance enhancement in your Raman spectra. How does resonance Raman spectroscopy differ from so-called normal Raman spectroscopy? The primary difference is that the scattering strength of those Raman active vibrational modes associated with the electronic transition are greatly enhanced, up to 10^6 times the signal strength observed when performing normal Raman spectroscopy. The presence of bands attributable to second-order overtone and combination modes in resonance Raman spectra is explained.

David Tuschel

Raman spectroscopists are aware of the fact that they have a choice of excitation wavelengths. A frequent question that new users have when acquiring a Raman spectrometer is "What excitation wavelengths will I need to perform Raman spectroscopy?" Usually, the choice of excitation wavelength is dictated by a desire to avoid absorption and subsequent fluorescence from the sample that can overwhelm the Raman signal. However, in those instances where fluorescence does not obscure the Raman spectrum, there can be real benefits to choosing an excitation wavelength that couples to an electronic transition or photon absorption of the material. When that is done, we say that the excitation wavelength is in resonance with an electronic transition, and the result can be resonance enhanced Raman spectra.

Resonance Raman spectroscopy cannot be described properly without invoking quantum mechanics and some mathematically complicated concepts in chemical physics. A detailed explanation of resonance Raman spectroscopy is beyond the scope of this installment. We encourage you to consult these good references should you want that level of detail (1–7). How does resonance Raman spectroscopy differ from so-called normal Raman spectroscopy? The primary difference is that the scattering strengths of those Raman active vibrational modes associated with the electronic transition are greatly enhanced, up to 10^6 times the signal strength observed when performing normal Raman spectroscopy. One immediate consequence of that phenomenon is that a resonance Raman spectrum can appear quite different from a normal or nonresonant Raman spectrum, because of the differences in relative intensities of the Raman bands.

Most users of Raman instrumentation are aware of the fact that the Raman spectrum of a material will appear the same even if different excitation wavelengths are used. The band positions and their relative intensities do not change as a function of the excitation wavelength if one incorporates a correction for the wavelength dependent instrument response function of the spectrometer. The wavelength independence of the Raman spectrum is true insofar as no absorption occurs for any of the laser excitation wavelengths. The absence of absorption is the condi-

tion associated with normal Raman spectroscopy. However, if the excitation wavelength is in resonance with an electronic transition of the sample, then enhancement of the signal strength of some Raman bands can occur. Consequently, the resonance Raman spectrum can appear quite different from the normal Raman spectrum because of the sometimes very significant differences in relative intensities. The band positions in *molecular* resonance Raman spectroscopy do not in general vary with excitation wavelength because local vibrational modes are the origin of Raman scattering. However, the situation is different for phonons in solid state materials. The coupling of phonons of different energies throughout the Brillouin zone to the electronic transition can lead to excitation wavelength dispersion, that is the dependence of the Raman band position on excitation wavelength.

The purpose of this installment of "Molecular Spectroscopy Workbench" is to provide you with an overview of the chemical physics of resonance Raman spectroscopy, present and discuss some examples of resonance Raman spectra, and discuss those things to be alert to in recognizing resonance enhancement in your Raman spectra. The first distinction that we want to make is between absorption and a scattering phenomenon. An electronic transition from the ground to a real excited state takes place on the order of 10^{-13} s or less. Once the electron is in the excited state, the molecule has time to rearrange or adjust its nuclear configuration to stabilize the energy before losing it through emission (fluorescence) or inter-nuclear collisions. Vibrational transitions occur on a time scale of approximately 10^{-9} s, and so we might say that a lot of time will pass following the initial absorption and transitions to various vibrational states within the excited electronic state, also known as *vibronic states*. After vibrational relaxation to the ground vibrational state of the excited electronic state has occurred, a photon

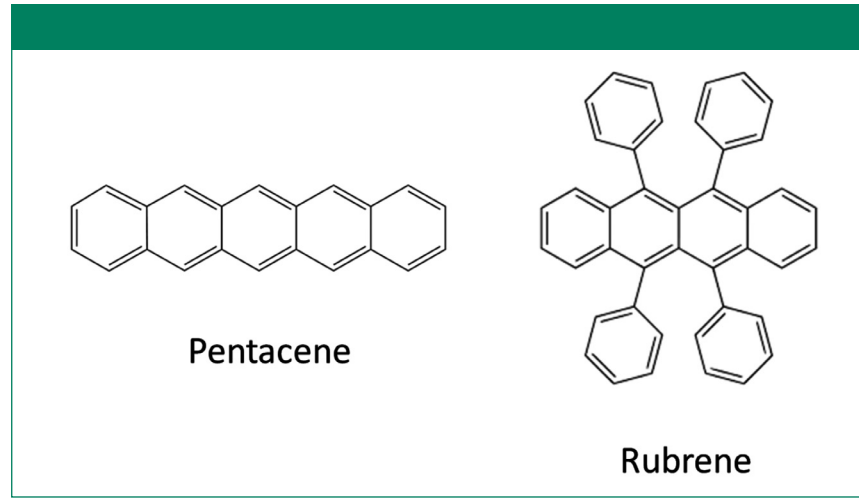

Figure 1: Molecular structures of pentacene and rubrene.

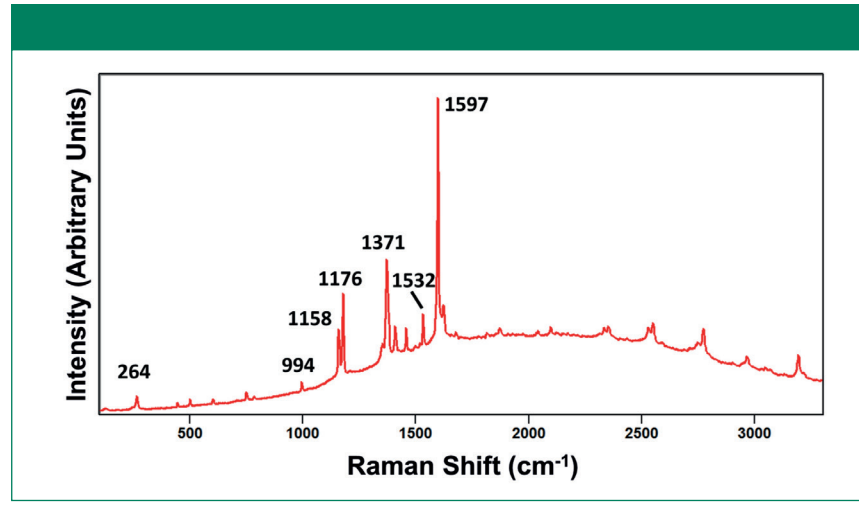

Figure 2: Raman spectrum obtained from a grain of pentacene using 633 nm excitation.

can be emitted through fluorescence or the molecule can return to the ground state through radiationless decay. Light scattering, including Raman scattering, is a fast process taking place on a time scale of 10^{-12} to 10^{-13} s. That difference in time scales between Raman scattering and fluorescence (10^{-9} s or greater) is the basis for being able to acquire Raman spectra without interfering fluorescence through time-resolved Raman spectroscopy.

Further to our discussion of time scales, we note that in resonance Raman spectroscopy the atoms don't have time to adjust to new equilibrium positions of their excited state as they do following absorption. Normal and resonance Raman scattering processes are fast and occur from a distorted structure formed by the mixing of the ground and excited states. In those relatively few (one in 10^6 to 10^8 incident photons) instances where a Raman photon is scattered the vibrational motion couples to the distorted excited state. In normal Raman spectroscopy the intermediate state is described as a virtual state, whereas in the case of resonance Raman spectroscopy that intermediate and distorted excited state corresponds to a real state of an electronic transition.

To understand the origins of the strengths of the various bands that constitute a Raman spectrum we consider the Kramers Heisenberg Dirac (KHD) equation.

$$(\alpha_{\rho\sigma})_{GF} = \frac{1}{h}\sum_{E} \frac{\langle F|r_\rho|E\rangle\langle E|r_\sigma|G\rangle}{\nu_{GE}-\nu_L-i\Gamma_E} + \frac{\langle E|r_\rho|G\rangle\langle F|r_\sigma|E\rangle}{\nu_{EF}+\nu_L-i\Gamma_E} \quad (1)$$

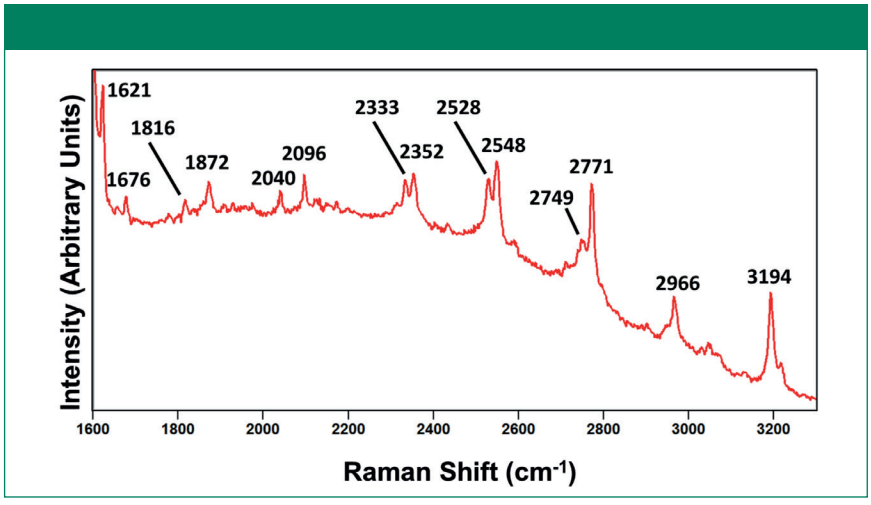

Figure 3: Raman spectrum obtained from a grain of pentacene using 633 nm excitation.

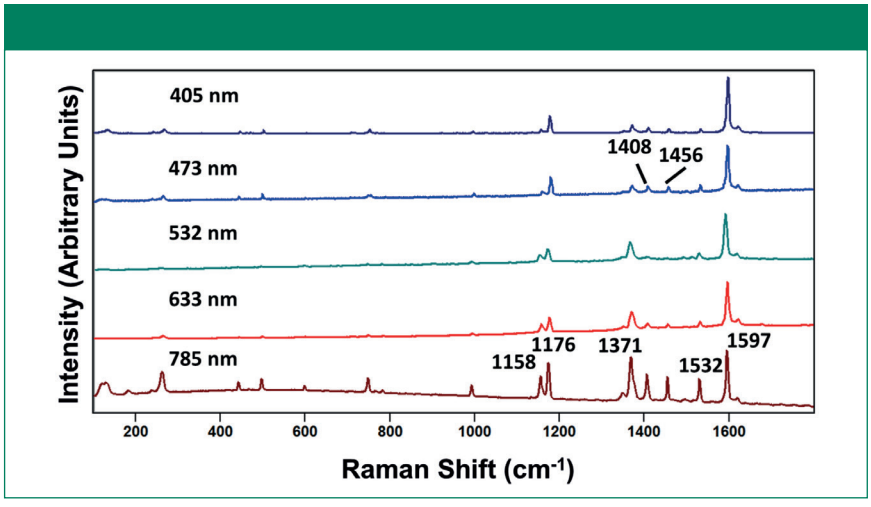

Figure 4: Raman spectra obtained from grains of pentacene using various excitation wavelengths.

The Raman polarizability is given by the term $(\alpha_{\rho\sigma})_{GF}$ where ρ and σ are the polarizations of incident and Raman scattered light and the terms *G* and *F* correspond to the ground and final vibronic states of the molecule. The excited state is indicated by *E*, which will be virtual or real depending upon whether the frequency of the exciting radiation matches that of an electronic transition of the molecule. The polarization dependent dipole operator is given by either r_ρ or r_σ. The summation symbol indicates that the Raman polarizability is given by the sum of all of the vibronic states of the molecule. Planck's constant is given by *h*, and ν_{GE}, ν_{EF}, and ν_L are the frequencies of the ground to excited state transition, excited state to final state transition, and laser, respectively. The term $i\Gamma_E$ is a damping constant and is related to the lifetime and therefore the band width of the excited state.

Note that the frequencies of the laser and the transition from the excited to final state in the denominator of the second term are added, whereas the frequency of the laser is subtracted from that of the transition from the ground to excited state in the first term denominator. Therefore, the second term will always be smaller than the first term and we can neglect it in our consideration of Raman polarizability and signal strength. Considering then the numerator in the first term, we recognize an expression of a two photon process. Reading the expression of integrals in bra-ket notation in the customary fashion from right to left, the first term in the numerator describes the mixing of ground and excited vibronic states and the second term accounts for the mixing of the excited and final vibronic states. Hence, Raman scattering is a two photon process which explains why it is inherently weak. One may be tempted to think of the two terms in the numerator as being analogous to an absorption followed by emission but that is not correct. It is more appropriate to think of the integrals in the numerator as the mixing of ground, excited, and final states of an electronic configuration distorted by the electric field of the incident light.

Turning our attention to the denominator in the first term brings us to the root of resonance enhanced Raman spectroscopy as found in the KHD equation. The closer the laser frequency is to that of an electronic transition the smaller the denominator becomes leaving only the damping constant, $i\Gamma_E$. Were it not for the addition of the damping constant, the denominator could in principle go to zero when the laser frequency equaled that of the electronic transition and the Raman polarizability would go to infinity. Of course, that doesn't happen and actual resonance enhancements over normal Raman scattering are typically 10^4 to 10^6. We stated earlier that the Raman polarizability depended upon the sum of the mixing of all of the ground, excited, and final vibronic states. However, when the laser excitation frequency matches that of a transition to a real electronic state rather than a virtual state, the resonance condition obtains, and the interaction described by the KHD expression is for that one resonance state and not the sum of all states.

Those Raman active vibrational modes associated with the electronic transition will then experience a significant increase of their vibrationally modulated polarizability and enhancement of their Raman scattering. The result of the enhance-

ment of those specific modes can be a Raman spectrum that appears different from the normal Raman spectrum of the same compound because of the different relative intensities of the bands. In addition, bands attributable to overtones and combination modes that are not seen in a normal Raman spectrum can become quite intense. Readers may be aware of the fact that the Raman spectrum normally comprises only the fundamental vibrational modes. However, using an excitation wavelength that couples to an electronic transition can give rise to the appearance of overtones to the 11th harmonic (2).

Matters can become even more complicated when the resonance condition occurs in solid state materials. Selection rules dictate that for first-order Raman scattering only those phonons at the Brillouin zone center will be Raman active. That is not the case for second-order Raman scattering involving overtones or combination modes. In second-order Raman scattering, all the phonons throughout the Brillouin zone can be Raman active. For example, that is why the 2TO band at approximately 950 cm^{-1} in the Raman spectrum of silicon (Si) is so much broader than that of the first-order optical mode at 520 cm^{-1}. Under the resonance condition, coupling of phonons of different energies within the Brillouin zone can lead to a change in the peak position of multiphonon Raman scattering depending upon the excitation wavelength (8).

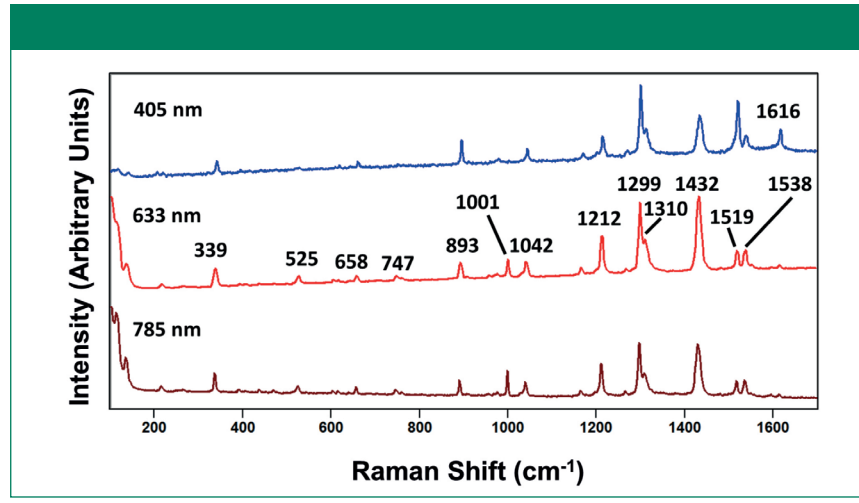

Figure 5: Raman spectra obtained from grains of rubrene using various excitation wavelengths.

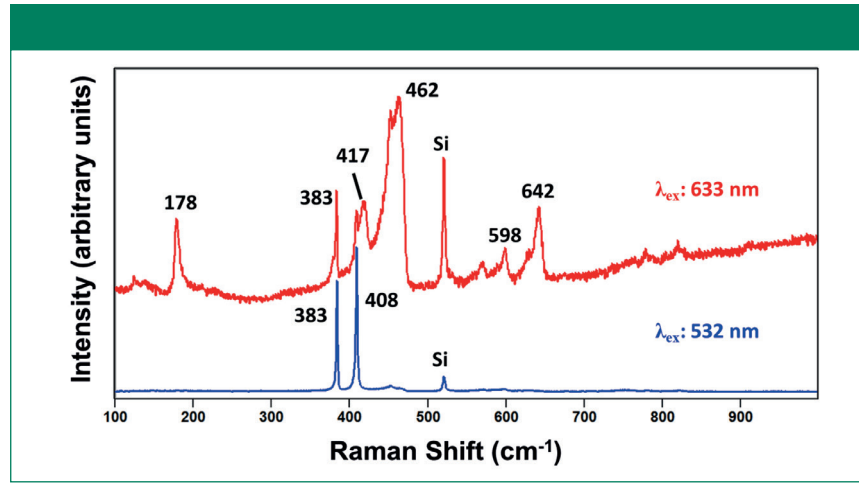

Figure 6: Raman spectra of 2D MoS2 taken at the same location with different excitation wavelengths.

Resonance Raman Spectroscopy of Pentacene and Rubrene

Pentacene and rubrene are two compounds of great interest in the world of molecular electronics and are solids at room temperature. Both compounds are aromatic, consisting entirely of phenyl groups, and are colored. Their molecular structures are shown in Figure 1. Rubrene has a bright reddish orange color and pentacene appears almost black. The rubrene grains have a glow to them under fluorescent room lighting and so their reddish orange color can probably be attributed to a combination of absorption of blue-green light and fluorescence of reddish-orange light. That these compounds absorb light in the visible region of the spectrum makes them good candidates for resonance Raman spectroscopy.

A resonance Raman spectrum of pentacene acquired using 633 nm excitation is shown in Figure 2. How do we know that the spectrum is resonantly enhanced? Our first clue is the appearance of Raman bands in the region between 1800 and 3000 cm^{-1}. The highest energy bands in the fingerprint region will be due to aromatic ring vibrational modes at approximately 1600 cm^{-1}. There are no saturated portions of the molecule and so we would not expect to see C-H stretching modes below 3000 cm^{-1}. Raman bands from aromatic C-H stretching should appear at energies greater than 3000 cm^{-1}, which do appear in this spectrum. So how do we account for the appearance of bands between 1800 and 3000 cm^{-1}? These bands can be attributed to the resonantly enhanced second-order combinations and overtones that we discussed in the previous section. No fundamental vibrational modes of pentacene would be expected in this portion of the spectrum. The most prominent bands in the spectrum appear at 1158, 1176, 1371, 1532 and 1597 cm^{-1}. The first four of these bands have been assigned to the A_g symmetry species and the 1597 cm^{-1} band to the B_{3g} symmetry species (9–10). It is generally accepted that totally symmetric A_g symmetry species

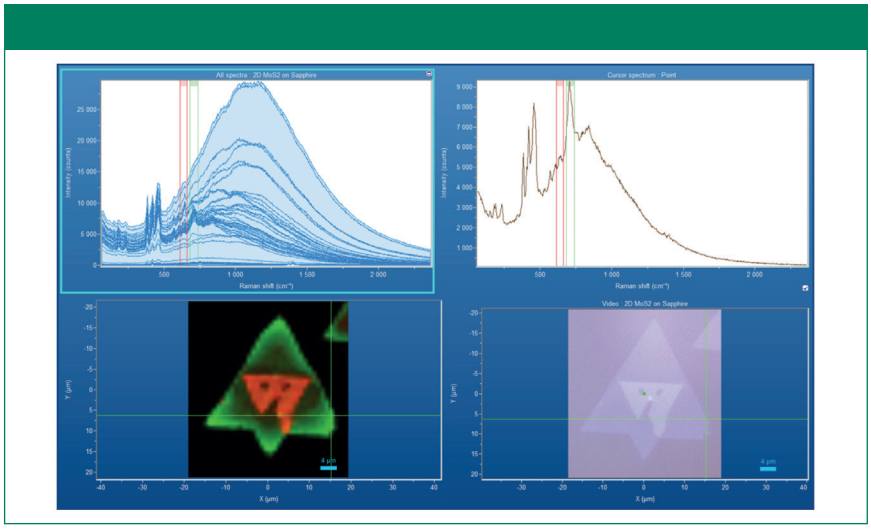

Figure 7: Raman hyperspectral data set (upper left) of 2D MoS_2. Reflected white light image appears in lower right corner. The color coded resonance Raman image in the lower left hand corner corresponds to the green and red brackets appearing in the hyperspectral data set and cursor spectrum in the upper right corner.

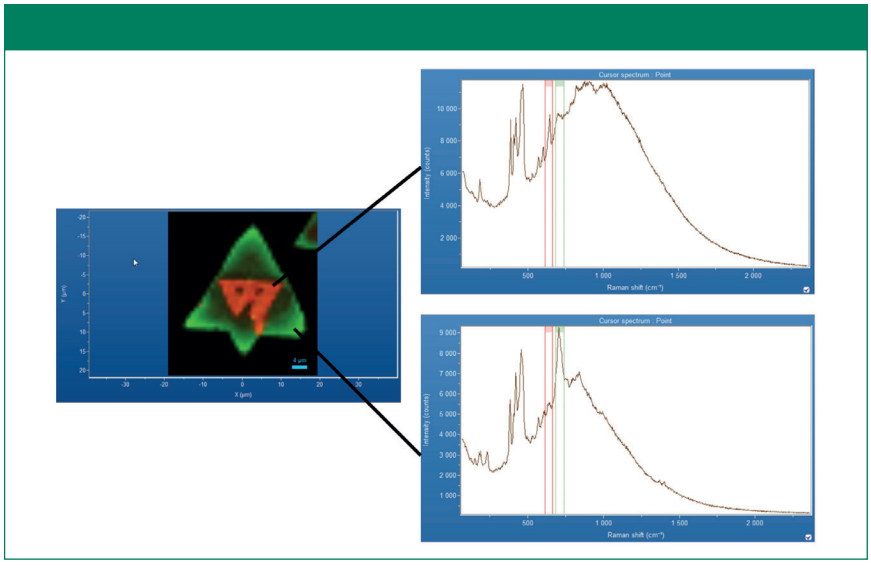

Figure 8: Color coded resonance Raman image (left) of 2D MoS_2. Raman spectra on the right are from the locations on the image indicated by the connecting lines.

that manifest resonance enhancement do so through a Franck-Condon coupling. There are other types of vibronic coupling to describe resonance enhancement, but those very detailed and mathematical explanations are beyond the scope of this installment. Assignments of the symmetry species that undergo resonance enhancement can often help in understanding the electronic transition and explaining the coupling between specific vibrational modes and the electronic transition.

An expanded view of that portion of the Raman spectrum consisting of overtones and combination modes is shown in Figure 3. The peak at 3194 cm^{-1} can be attributed to aromatic C-H stretching. However, all of the other bands in Figure 3 can only be assigned to second-order overtones and combination modes and not to any fundamental vibrational modes of pentacene. Raman spectroscopists need to be aware of this aspect of resonance Raman spectroscopy lest they attempt to assign these bands to particular functional groups, leading to an incorrect construction of a molecular structure. Furthermore, you can see the risks of basing a library search on a resonance Raman spectrum. All of the spectra that constitute a spectral database can be expected to consist of normal (nonresonant) Raman spectra. It is unlikely that you would obtain an accurate match and identification for the spectrum in Figure 2 by searching a Raman database if it is comprised of normal Raman spectra.

Another aspect of resonance Raman spectroscopy is the excitation profile or differences in the Raman spectra as a function of excitation wavelength. Normally, the peak positions will not change with excitation wavelength for molecular resonance Raman spectroscopy. However, as we explained earlier, a dependence of band position on excitation wavelength can be observed in spectra of solid state materials where phonons of different energies throughout the Brillouin zone couple to the electronic transition. What do change are the relative intensities of the bands. A profile of Raman spectra of pentacene acquired using 405, 473, 532, 633, and 785 nm excitation is shown in Figure 4. The spectrum acquired with 785 nm excitation can be considered a normal Raman spectrum because the energy of 785 nm light is below the bandgap of pentacene. All of the other excitation wavelengths fall within the absorption spectrum of pentacene and therefore yield resonantly enhanced Raman spectra (11). Although absorption occurs for all of the other laser excitation wavelengths, they do not all couple to the same electronic transition. Note how the Raman spectra excited at 405 and 473 nm are nearly identical, thereby indicating that those excitation wavelengths couple to the same electronic transition. Using a longer excitation wavelength at 532 nm, we see definite changes in the relative intensities of the bands. In particular, the strengths of the bands at 1158 and 1371 cm^{-1} have increased relative to their counterparts in the spectra excited at 405 and 473 nm. Also, the

bands at 1408 and 1456 cm^{-1} have diminished in relative strength at 532 nm excitation. Furthermore, all of the bands below 1000 cm^{-1} are now extremely weak and can barely be observed plotted on a scale normalized to the most intense band. This was not the case for the spectra obtained at 405 and 473 nm excitation. At 633 nm excitation, the spectrum is similar to that obtained with 532 nm excitation, but we observe a small recovery of the strengths of the 1408 and 1456 cm^{-1} bands. Finally, at 785 nm excitation we observe a very different Raman spectrum with respect to relative intensities because at this wavelength we are now out of resonance.

The dependence of Raman band strength on the excitation wavelength as observed in Figure 4 and discussed above can seem puzzling without reference to the absorption spectrum of pentacene. An absorption spectrum of a 150 nm thick polycrystalline film of pentacene is shown in Figure 2 of reference (11). That spectrum reveals absorption at wavelengths shorter than 740 nm with absorption maxima at approximately 540, 580, 630 and 670 nm. We can then infer with reference to that absorption spectrum and its multiple absorption maxima that we are coupling into different electronic transitions with the laser wavelengths available to us. The 405 and 473 nm laser light couples to a transition well above the band gap and the 532 and 633 nm laser excitations couple to the absorption maxima at 540 and 630 nm, respectively. The excitation profile of pentacene offers a good example of the complexity of resonance Raman spectroscopy when the absorption spectrum of a compound has multiple electronic transitions into which one can couple using different laser excitation wavelengths.

Rubrene is another aromatic compound that has been extensively studied for its use in molecular electronics. It too is colored, and the absorption spectrum of its solid form extends from the UV to approximately 590 nm (12). The absorption spectrum manifests maxima at approximately 440, 465, 495 and 535 nm. Several of the absorption maxima are well placed for the laser wavelengths available to us. However, rubrene (like pentacene) is a strong fluorophore and the emission from this compound overwhelms the Raman scattering when using 473 and 532 nm excitation. No Raman bands could be detected superimposed on the very strong fluorescent background. The Raman spectra that we were able to acquire using 405, 633 and 785 nm excitation are shown in Figure 5. The spectra acquired at 633 and 785 nm excitation are nearly identical as we might expect. This is because there is little if any absorption at these wavelengths and so there is no resonance enhancement of the Raman scattering. These excitation wavelengths have energies below the bandgap of rubrene. The Raman spectrum acquired using 405 nm excitation appears distinctly different from the two excited with 633 and 785 nm laser light. Here we observe the effects of resonance enhancement. A band appears at 1616 cm^{-1} that is very weak in the spectra acquired with 633 and 785 nm excitation. Also, you can see that the relative intensities of the spectrum excited with 405 nm light differ from those excited at 633 and 785 nm. Identification of the site symmetry species of the prominent bands in the 405 nm excited spectrum reveals something very interesting. All of the moderate to strong bands with the exception of one are of symmetry species A_g, based upon the assignments of Weinberg-Wolf and coworkers (13). The exceptional band is at 1519 cm^{-1}, which has been assigned to symmetry species B_g. Thus, all but one of the resonance enhanced Raman bands are totally symmetric modes belonging to the symmetry species A_g. This observation would lead us to conclude that the resonance enhancement at 405 nm excitation is through a Franck-Condon coupling mechanism.

You can see the risks of basing a library search on a resonance Raman spectrum.

Coupling to an Exciton in 2D MoS_2

Resonance Raman spectroscopy has played an important role in the characterization of two dimensional (2D) crystals. These novel materials are not just small portions of the bulk materials carrying the same properties as those of the three dimensional kind. Rather, their physical, electronic, and spectral characteristics can be significantly different. Specifically, molybdenum disulfide (MoS_2) in its bulk form is an indirect bandgap semiconductor, whereas in its monolayer to few-layer forms it becomes a direct bandgap semiconductor (14). Splendani and coworkers have studied an exfoliated MoS_2 monolayer and a few-layer flakes by photoluminescence and have observed direct excitonic transitions (15). By exciting with 532 nm laser light they have observed broad photoluminescence centered at 627 and 677 nm, whereas these emissions are completely absent when illuminating bulk MoS_2. The room temperature bandgap of bulk MoS_2 is approximately 1.7 eV (corresponding to 730 nm) with complex excitonic features between 1.7 and 2.5 eV (16).

The crystalline structure of 2D MoS_2 belongs to the D_{6h} crystal class, and factor group analysis predicts one A_{1g}, one E_{1g} and two E_{2g} Raman active modes (16-22). The symmetry assignments and corresponding Raman band positions for the fundamental (first-order) phonon modes of bulk hexagonal MoS_2 are: E_{1g} (286 cm^{-1}), E^1_{2g} (383 cm^{-1}), A_{1g} (408 cm^{-1}) and E^2_{2g} (32 cm^{-1}). Furthermore, it is important to remember that some visible wavelengths of the laser light used to excite Raman scattering correspond

to energies of MoS_2 electronic transitions. The absorption spectrum of MoS_2 reflects the band gap of 1.7 eV, but it also manifests fine structure with narrow absorption peaks at 1.9 eV (653 nm) and 2.1 eV (590 nm) related to d-to-d orbital transitions split by spin-orbit coupling and designated A1 and B1 excitons, respectively (16,23). Consequently, one can observe an excitation wavelength dependence of the first-order Raman band intensities as well as the appearance of Raman bands assigned to second-order overtone and combination modes when the laser excitation is of a wavelength that couples into these excitonic transitions (16, 20, 22-23).

The Raman spectra of 2D MoS_2 depend upon the excitation wavelength. Spectra acquired at the same location from the interior of a MoS_2 few-layer flake on a Si substrate with different excitation wavelengths are shown in Figure 6. The spectrum acquired with 532 nm excitation is typical of those reported in the literature; it consists primarily of the E^1_{2g} band at 383 cm^{-1} and the A_{1g} band at 408 cm^{-1} as well as the Si substrate Raman band at 520 cm^{-1}. In contrast, the spectrum generated with 633 nm excitation is striking insofar as it consists of the same first-order bands and those due to overtones and combination modes. Remember that the absorption spectrum of MoS_2 contains fine structure with narrow absorption peaks at 1.9 eV (653 nm) and 2.1 eV (590 nm) related to d-to-d orbital transitions split by spin-orbit coupling and designated A1 and B1 excitons, respectively (16, 23). Consequently, the 633 nm excitation couples into the A1 transition producing a resonance enhancement of all of the additional modes observed in Figure 6. All of the bands in the spectrum excited with 633 nm light can be accounted for and have previously been assigned (16, 20, 23-24).

The assignment of symmetry species of these bands reveals the complexity that can sometimes emerge in the resonance Raman spectroscopy of solid state materials. For example, the band at 178 cm^{-1} is a combination of an A_{1g} and a longitudinal acoustic (LA) mode at the M point of the Brillouin zone (A_{1g}(M) LA(M)) (24). The band at 417 cm^{-1} has been designated a so-called "b" mode involving a polariton and manifesting wavelength dependent dispersion (25-26). The bands at 462, 598, and 642 cm ^{1} have been assigned to the symmetry species $A_{2u}(\Gamma)$ or $E_{1g}(\Gamma)$ + XA, E^1_{2g}(M) + LA(M), and A_{1g}(M) + LA(M), respectively. You can see from these symmetry species and band assignments that we have departed the more familiar territory of molecular spectroscopy and entered the more complex world of solid state physics. The band positions in *molecular* resonance Raman spectroscopy do not in general vary with excitation wavelength because local vibrational modes are the origin of the Raman scattering. However, the situation is different for phonons in solid state materials. The coupling of phonons of different energies throughout the Brillouin zone to the electronic transition can lead to excitation wavelength dispersion, that is the dependence of the peak position on excitation wavelength. Furthermore, the resonantly enhanced second-order modes are no longer restricted to only those phonons at the Brillouin zone center (Γ) as are the first-order fundamental modes. Phonons throughout the Brillouin zone and even those modes that by symmetry (e.g., $A_{2u}(\Gamma)$) should not be Raman active can appear through resonance in the Raman spectrum.

The structure of 2D MoS_2 often varies spatially and the most prominent changes appear at the sample edges. Resonance Raman imaging of these 2D crystals is complementary to photoluminescence imaging and offers a means of imaging the spatially varying electronic structure. The results of resonance Raman mapping of 2D MoS_2 crystals on a Si substrate using 633 nm excitation are shown in Figure 7. The Raman data were acquired using a 100 x Olympus objective and by moving the stage in 1 µm spatial increments over an area of approximately 40 µm x 40 µm. A 300 grove per mm grating was used in order to capture both Raman scattering and photoluminescence in one spectral acquisition without the need for moving the grating to stitch regions together. The hyperspectral data set appearing in the upper left corner of Figure 7 consists of all the spectra acquired during mapping. You can see from the variation in the photoluminescence of those spectra that the electronic properties of the crystal varied spatially. A reflected white light image of the sample appears in the lower right hand corner and a resonance Raman image corresponding to the reflected light image appears to its left. The upper right hand plot is of the single spectrum associated with the cross hair location in the Raman and reflected light images.

The resonance Raman image is actually a rendering of signal strength for a particular Raman band as a function of position on the sample. In this case, the resonance Raman image is rendered through a color coded plot of Raman signal strength of the corresponding color bracketed Raman shift positions in the two upper traces. Peak intensities were measured incorporating a baseline to remove any contribution from the underlying photoluminescence. Therefore, the spectral image in Figure 7 is strictly a resonance Raman image.

The red brackets surround the second-order MoS_2 Raman band at 642 cm^{-1} (A_{1g}(M) + LA(M)). This band appears only in the two trilayer MoS_2 crystal and is absent in the single trilayer MoS_2. Consequently, only the two trilayer structure in the center of the MoS_2 crystal appears red. The green bracket covers the second-order Raman scattering near 706 cm^{-1}, which is assigned to the second-order mode $A_{1g}(\Gamma) + E_{1g}(\Gamma)$ at the Brillouin zone center. This second-order mode is prominent in the single trilayer MoS_2 spectrum because of resonance enhancement. Thus, these two resonantly enhanced Raman bands offer a means of easily differentiating single from double trilayer MoS_2, thereby producing resonance Raman images with excellent contrast based on the number of 2D layers. Note how well the resonance Raman image cor-

responds to the reflected white light image in which the hue and degree of white light reflectance depend upon the number of MoS_2 trilayers.

Spectra from the two trilayer structure in the crystal center and from the single trilayer perimeter are shown in Figure 8. Note how intense the green color associated with the single trilayer 706 cm^{-1} band is near the perimeter but is dimmer in the interior of the crystal. This strong resonance Raman response at the perimeter inversely correlates with the diminished photoluminescence regularly observed at the crystal's edge. Also, the second-order MoS2 Raman band at 642 cm^{-1} (A_{1g}(M) + LA(M)) is much stronger in the two trilayer crystal where one also observes differences in photoluminescence band shape and strength relative to those from a single trilayer. Thus, the combination of resonance Raman and photoluminescence imaging allows investigators to more thoroughly characterize the electronic properties of these new and technologically important materials.

Conclusion

Resonance Raman spectroscopy cannot be described properly without invoking quantum mechanics and some mathematically complicated concepts in chemical physics. A detailed explanation of resonance Raman spectroscopy is beyond the scope of this installment and so we provided an overview of the phenomenon. The primary difference between normal and resonance Raman spectroscopy is that the scattering strengths of those Raman active vibrational modes associated with the electronic transition is greatly enhanced, up to 10^6 times the signal strength observed when performing normal Raman spectroscopy. Resonance Raman spectra of pentacene and rubrene were presented and discussed. These spectra demonstrate that second-order Raman scattering from overtones and combination modes can be resonantly enhanced to appear in resonance Raman spectra whereas they are absent in normal Raman spectra. The assignment of vibrational mode symmetry species was shown to be important in understanding the resonance mechanism. Resonance Raman spectra and images of 2D MoS_2 were also shown and discussed. It was shown that two resonantly enhanced Raman bands offer a means of easily differentiating single from double trilayer MoS2, thereby producing resonance Raman images with excellent contrast based on the number of 2D layers. The combination of resonance Raman and photoluminescence imaging allows investigators to more thoroughly characterize the electronic properties of these new and technologically important materials.

References

(1) R.J.H. Clark and T.J. Dines, *Angew. Chem. Int. Ed.* **25**, 131-158 (1986).

(2) R.J.H. Clark and B. Stewart, *Struct. Bond.* **36**, 1-80 (1979).

(3) D.P. Strommen and K. Nakamoto, *J. Chem. Educ.* **54**, 474-478 (1977).

(4) E. Smith and G. Dent, Chapter 4: *Resonance Raman Scattering in Modern Raman Spectroscopy: A Practical Approach* (John Wiley & Sons, Chichester, England, 2005), pp. 93-112.

(5) A.B. Myers, *Chem. Rev.* **96**, 911-926 (1996).

(6) S.A. Asher, *Analyt. Chem.* **65**, 59A-66A (1993).

(7) S.A. Asher, *Analyt. Chem.* **65**, 201A-210A (1993).

(8) P.Y. Yu and M. Cardona, *Fundamentals of Semiconductors: Physics and Materials Properties* (Springer, Berlin, 1996), pp. 403-406.

(9) Y. Yamakita, J. Kimura and K. Ohno, *J. Chem. Phys.* **126**, 064904 (2007).

(10) K. Seto and Y. Furukawa, *J Raman Spectrosc.* **43**, 2015-2019 (2012).

(11) M.W.B. Wilson, A. Rao, B. Ehrler and R.H. Friend, *Acc. Chem. Res.* **46**, 1330-1338 (2013).

(12) P. Irkhin, A. Ryasnyanskiy, M. Koehler and I. Biaggio, *Phys. Rev. B* **86**, 085143 (2012).

(13) J.R. Weinberg-Wolf, L.E. McNeil, S. Liu and C. Kloc, *J. Phys. Condens. Matter* **19**, 276204 (2007).

(14) K.F. Mak, C. Lee, J. Hone, J. Shan and T.F. Heinz, *Phys. Rev. Lett.* **105**, 136805 (2010).

(15) A. Splendiani, L. Sun, Y. Zhang, T. Li, J. Kim, C.-Y. Chim, G. Galli and F. Wang, *Nano Lett.* **10**, 1271-1275 (2010).

(16) A.M. Stacy and D.T. Hodul, *J. Phys. Chem. Solids* **46**, 405-409 (1985).

(17) J.R. Ferraro, *Appl. Spec.* **29**, 418-421 (1975).

(18) S. Jimenez Sandoval, D. Yang, R.F. Frindt and J.C. Irwin, *Phys. Rev. B* **44**, 3955-3962 (1991).

(19) T.J. Wieting and J.L. Verble, *Phys. Rev. B* **3**, 4286-4292 (1971).

(20) J.M. Chen and C.S. Wang, *Solid State Commun.* **14**, 857-860 (1974).

(21) S. Sugai and T. Ueda, *Phys. Rev. B* **26**, 6554-6558 (1982).

(22) D.O. Dumcenco, K.Y. Chen, Y.P. Wang, Y.S. Huang and K.K. Tiong, *J. Alloys Compounds* **506**, 940-943 (2010).

(23) B.C. Windom, W.G. Sawyer and D.W. Hahn, *Tribol. Lett.* **42**, 301-310 (2011).

(24) M. Placidi, M. Dimitrievska, V. Ezquierdo-Roca, X. Fontane, A. Castellanos-Gomez, A. Perez-Tomas, N. Mestres, M. Espindola-Rodriquez, S. Lopez-Marino, M. Neuschitzer, V. Bermudez, A. Yaremko and A. Perez-Rodriguez, *2D Mater.* **2**, 035006 (2015).

(25) K. Golasa, M. Grzeszczyk, R. Bozek, P. Leszczynski, A. Wysmolek, M. Potemski and A. Babinski, *Solid State Commun.* **197**, 53-56 (2014).

(26) B. Chakraborty, H.S.S. Ramakrishna Matte, A.K. Sood and C.N.R. Rao, *J. Raman Spectrosc.* **44**, 92-96 (2013).

David Tuschel is a Raman Applications Scientist at Horiba Scientific, in Piscataway, New Jersey, where he works with Fran Adar. David is sharing authorship of this column with Fran. He can be reached at: SpectroscopyEdit@UBM.com

For more information on this topic, please visit: www.spectroscopyonline.com/adar